



Slip of styrene–butadiene rubbers: The effects of pressure and viscous heating.

Downloaded from: <https://research.chalmers.se>, 2025-12-04 22:36 UTC

Citation for the original published paper (version of record):






Georgantopoulos, C., Zhang, Z., Pollard, M. et al (2024). Slip of styrene–butadiene rubbers: The effects of pressure and viscous heating.. *Physics of Fluids*, 36(1). <http://dx.doi.org/10.1063/5.0191839>

N.B. When citing this work, cite the original published paper.

RESEARCH ARTICLE | JANUARY 30 2024

Slip of styrene–butadiene rubbers: The effects of pressure and viscous heating **FREE**

Special Collection: [Tanner: 90 Years of Rheology](#)

Christos K. Georgantopoulos (Χρήστος Κ. Γεωργαντόπουλος); Ziyue Zhang (张子越) ; Michael A. Pollard; Andrea Causa; Roland Kádár ; Manfred Wilhelm ; Evelyne van Ruymbeke ; Savvas G. Hatzikiriakos (Σάββας Γ. Χατζηκυριάκος)  




Physics of Fluids 36, 013127 (2024)

<https://doi.org/10.1063/5.0191839>




CrossMark



Physics of Fluids

Special Topic: K. R. Sreenivasan:
A Tribute on the occasion of his 75th Birthday

Submit Today



Slip of styrene-butadiene rubbers: The effects of pressure and viscous heating

Cite as: Phys. Fluids **36**, 013127 (2024); doi: [10.1063/5.0191839](https://doi.org/10.1063/5.0191839)

Submitted: 16 December 2023 · Accepted: 3 January 2024 ·

Published Online: 30 January 2024








View Online



Export Citation



CrossMark

Christos K. Georgantopoulos (Χρήστος Κ. Γεωργαντόπουλος),¹ Ziyue Zhang (张子越),²  Michael A. Pollard,² Andrea Causa,³ Roland Kádár,⁴  Manfred Wilhelm,¹  Evelyne van Ruymbeke,⁵  and Savvas G. Hatzikiriakos (Σάββας Γ. Χατζηκυριάκος)^{2,a)} 

AFFILIATIONS

¹Karlsruhe Institute of Technology (KIT), Institute of Chemical Technology and Polymer Chemistry (ITCP), Engesserstraße 18, 76131 Karlsruhe, Germany

²Department of Chemical and Biological Engineering, University of British Columbia, 2360 East Mall, Vancouver, British Columbia V6T-1Z3, Canada

³Pirelli Tyre S. p. A., R&D, Viale Piero e Alberto Pirelli 25, 20126 Milan, Italy

⁴Department of Industrial and Materials Science, Division of Engineering Materials, Chalmers University of Technology, SE-412 96 Gothenburg, Sweden

⁵Bio- and Soft Matter, Institute of Condensed Matter and Nanosciences, Universite Catholique de Louvain, Croix du Sud 1, B-1348 Louvain-la-Neuve, Belgium

Note: This paper is part of the special topic, Tanner: 90 Years of Rheology.

^{a)} Author to whom correspondence should be addressed: savvas.hatzi@ubc.ca

ABSTRACT

During the processing of elastomeric compounds under high flow rates, significant pressure drops (10^6 – 10^8 Pa) are encountered. Under such conditions, the viscosity of these compounds is significantly affected by pressure and viscous heating. Moreover, strong flow rates may cause these systems to slip at the wall, violating the classical no-slip boundary condition of fluid mechanics. To determine the slip velocity by the well-known Mooney method, the effects of pressure and viscous heating should be considered. In this work, an experimental methodology is developed to determine the slip velocity of styrene-butadiene compounds in capillary flow corrected for the effects of pressure and viscous heating. First, the temperature increase due to viscous heating is measured during the extrusion process and accounted for in correcting the experimental data to infer the slip velocity. Consequently, the corrected experimental data for the effects of pressure and viscous heating are used to calculate the slip velocity from the deviation of the linear viscoelastic behavior (deviation from the Cox–Merz rule). The Mooney method is also used to confirm the calculated slip velocity of the elastomeric compounds.

Published under an exclusive license by AIP Publishing. <https://doi.org/10.1063/5.0191839>

I. INTRODUCTION

It is generally accepted that polymer melts, unlike Newtonian fluids, violate the classical no-slip boundary condition of Newtonian fluid mechanics and slip over solid surfaces.¹ One of the common tools to study the wall slip phenomenon is capillary rheometry by using the classical Mooney method.^{1,2} This technique requires the performance of capillary experiments with a series of capillary dies having the same length-to-diameter ratio, L/D , in order to keep constant the effect of pressure and different diameters, D . If slip occurs, the flow curves exhibit diameter dependence. The use of Mooney analysis to quantify the slip velocity for rubber compounds has been discussed in the literature^{3,4} with contradictory results. One could expect that the Mooney

method cannot be applied for all cases. Indeed, this has been noted by many researchers where in a Mooney plot (apparent shear rate vs the inverse of capillary diameter), the experimental data do not fall on a straight line.^{5–8} Unfortunately, such anomalies are ignored by researchers in the field, which may lead to inaccurate slip velocity calculations. An alternative way (used in the current study) is to use the deviation of the flow curve determined from capillary rheometry from the linear viscoelastic data, for cases where the Cox–Merz⁹ rule fails. It is noted that the Cox–Merz⁹ rule assumes that the magnitude of the complex viscosity $\eta^*(\omega)$ obtained by a rotational rheometer is equal to the shear viscosity $\eta(\dot{\gamma})$ by capillary rheometer, at the same values of the angular frequency ω (rad/s) and steady-state shear rate $\dot{\gamma}$ (s^{-1}),

respectively. Thus, $|\eta^*(\omega)| = \eta(\dot{\gamma})$ for $\dot{\gamma} = \omega$. Another version of the Cox–Merz rules has been suggested by Winter,¹⁰ where the steady-state shear stress $\sigma(\dot{\gamma})$ is compared to the magnitude of the complex shear modulus $|G^*(\omega)|$, $\sigma(\dot{\gamma}) = |G^*(\omega)|$ for $\dot{\gamma} = \omega$.

The classical Mooney² method neglects the viscous heating and pressure effects. According to Winter¹¹ and Cox *et al.*,¹² it is reasonable to expect that the effect of viscous heating is significant at sufficiently high shear rates. Specifically, Cox *et al.*¹² presented experimental results in which the temperature increases significantly inside the die due to viscous heating exhibiting dependence on the geometrical characteristics of the die (length-to-diameter ratio, L/D , and capillary die diameter, D). Cox *et al.*¹² investigated the flows of an acrylonitrile butadiene styrene (ABS) copolymer (Marbon & Kralastic HB) and a branched polyethylene (PE; DFDC 0506NT) using capillary rheometry. The ABS exhibited a temperature increase up to 20 °C in slit die flow (height $H=0.0475$ cm, width $W=0.4031$ cm, length $L=2.683$ cm, and $L/H=56.5$) and up to 60 °C in capillary die flow (diameter $D=0.318$ cm, length $L=9.53$ cm, and $L/D \sim 30$), with both experiments set up at $T=230$ °C. The branched PE exhibited a temperature increase up to 30 °C for an annular die [outer diameter $D_o=1.02$ cm, inner diameter $D_i=0.5$ cm, length $L=10.16$ cm, and $L/(D_o - D_i)=19.5$], with the extrusion temperature set at $T=200$ °C. Rosenbaum and Hatzikiriakos⁷ presented a detailed analysis of the dependency of viscous heating (temperature increase) in capillary extrusion for polypropylene (PP) samples. In particular, capillary experimental data obtained by using capillary dies with $L/D=10$, 40, and 70 having diameters of $D=0.508$, 0.762, and 1.270 mm, respectively, were analyzed. The main outcome of the study was that the radial temperature profile increases at the wall as the aspect ratio L/D increases. In addition, keeping constant the aspect ratio $L/D=40$ while varying the die diameter $D=0.508$, 0.762, and 1.270 mm, it was shown that the polymer flowing in the larger diameter exhibited the most intense temperature rising on the die wall due to higher volume and thus higher energy dissipation.⁷

The flow of filled rubber compounds and their detailed description of temperature increase during extrusion have not been analyzed extensively. Soltani and Sourki¹³ published a detailed parameter analysis of several carbon black (CB) grades and their influence on the viscous heating of rubber compounds.⁹ In addition, Heyer *et al.*¹⁴ presented temperature profiles obtained during the extrusion of styrene–butadiene rubber (SBR)-filled compounds at the extrusion temperature of 80 °C, reporting a temperature increase up to 40 °C depending on the shear rate.

In this work, an experimental methodology is developed in order to determine the slip velocity of styrene–butadiene compounds in capillary flow corrected for the effects of pressure and viscous heating. Flow in a long capillary die is used ($L/D=60$) where the pressure is high, causing significant viscous dissipation.¹⁵ The Denn model¹⁶ is used to estimate the theoretical pressure drop, taking into account the compressibility of the material; hence, the pressure-corrected wall shear stress is obtained. This is used to estimate the slip velocity decoupled from the effects of pressure and viscous heating.

II. MATERIALS AND EXPERIMENTAL METHODS

A. Materials

Three commercial styrene–butadiene rubbers, labeled as SBR A, SBR B, and SBR C, with different microstructure and similar molecular

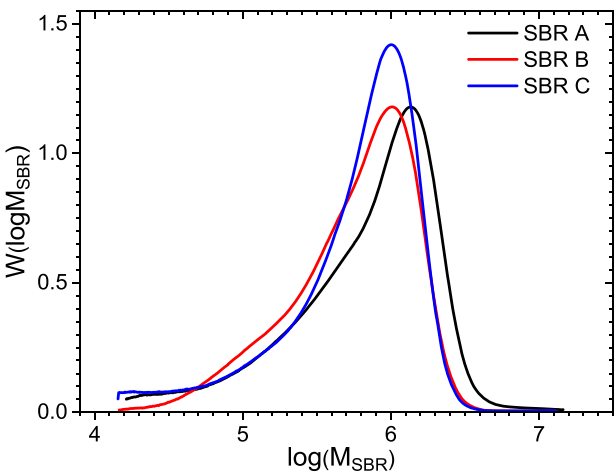


FIG. 1. The molar mass distribution of the three SBR samples listed in Table I.

weight distribution (MWD) are investigated in this work. The materials were provided by Pirelli Tyre S. p. A. (Milan, Italy). The molecular characterization of the investigated samples was carried out by size exclusion chromatography (SEC) in order to determine the molecular weight distribution and other details of their molecular architecture, i.e., linear vs branched. Figure 1 presents the molecular weight distribution of the investigated samples. Table I lists the molecular characteristics of the samples. The SBR A has the highest average weight of molecular weight, $M_w=1048$ kg mol⁻¹. The molar mass dispersity, \bar{D} , of the samples is also listed in Table I. All possess moderate dispersion ($\bar{D}=2.5\text{--}3.1$). Finally, the chemical composition in weight percentage (wt.%) and the glass transition temperature of the investigated SBR samples are summarized in Table II.

TABLE I. Molecular weight characteristics of the investigated SBR polymers.

Compound	M_n (kg mol ⁻¹)	M_w (kg mol ⁻¹)	M_z (kg mol ⁻¹)	\bar{D} (-)
SBR A	385	1048	1501	2.7
SBR B	317	791	1232	2.5
SBR C	264	817	1244	3.1

TABLE II. Chemical composition and the glass transition temperature of the investigated SBR samples.

Compound	Styrene (wt. %)	Butadiene		T_g (°C)
		Butadiene 1.2 (wt. %)	1,4 (cis and trans) (wt. %)	
SBR A	40	25	35	-33
SBR B	25	28	47	-47
SBR C	24	25	51	-51

B. Experimental methods

The linear viscoelastic behavior of the SBR compounds was characterized using a stress-controlled rotational rheometer (Anton Paar, MCR 502) equipped with a 25-mm diameter parallel plate geometry. A convection oven was used for temperature control with accuracy of $\pm 0.1^\circ\text{C}$. The linear viscoelastic region was determined by a strain amplitude sweep ranging from $\gamma = 0.1\%$ to 100% at constant oscillatory frequency $\omega = 1\text{ Hz}$ and reference temperature of $T = 100^\circ\text{C}$. Oscillatory frequency sweeps were conducted at an applied strain of $\gamma = 5\%$ over a range of frequencies $\omega = 0.01\text{--}100\text{ rad}\cdot\text{s}^{-1}$ at temperatures in the range of $50\text{--}170^\circ\text{C}$. The time-temperature superposition (tTS) principle was applied to construct master curves of storage $G'(\omega)$ and loss $G''(\omega)$ moduli. All rheology data were analyzed using the IRIS RheoHub software.¹⁷

The slip of compounds at high shear rates were studied by using a pressure driven Instron capillary rheometer equipped with a barrel having a diameter of 0.9525 cm . The diameter and length of the capillary die were $D = 1.78\text{ mm}$ and $L = 106.8\text{ mm}$ ($L/D = 60$). By using a die with the aspect ratio $L/D = 60$, the Bagley correction is insignificant and thus neglected.¹⁵ The Rabinowitsch-Weissenberg¹⁸ correction was applied to the data to obtain the true viscosity of the samples in order to compare them with complex viscosity data obtained from the parallel plate rheometer, i.e., check the Cox-Merz rule.⁹

III. MODELING OF CAPILLARY FLOW WITH VISCOUS HEATING

To consider the effects of pressure and viscous heating on the shear rate-dependent viscosity, two steps are followed. First, the pressure influence of viscosity has to be estimated by considering the two conditions according to Denn:¹⁶

- (i) In cylindrical coordinates, the only non-zero velocity component is the axial velocity, $V_z(r) = (2Q/\pi R^2) [1 - (r/R)^2]$. In other words, the small two-dimensional effects due to polymer compressibility and pressure-dependent viscosity are neglected. $R/L < (1 - \beta\Delta p_0)/\beta\Delta p_0 < 1/\beta\Delta p_0$, implying insignificant two-dimensional effects where V is the average velocity in the capillary die ($V = Q/\pi R^2$), Q is the volumetric flow rate, R is the radius of the capillary die, and Δp_0 is the experimental pressure drop measured by capillary rheometry. The compressibility factor (pressure dependency of viscosity) for SBR is about $\beta = 6 \times 10^{-10}\text{ Pa}^{-1}$.¹⁹ Once these conditions are satisfied, Denn¹⁶ suggested the following equation to estimate the pressure drop, corrected for the influence of compressibility:

$$\Delta p = -\frac{1}{\beta} \ln(1 - \beta\Delta p_0) + \frac{1}{\beta} \ln\left(\frac{2 - 2\sqrt{1 - X^2}}{X^2}\right) + \frac{1}{2\beta} \left(1 - \frac{2 - 2\sqrt{1 - X^2}}{X^2}\right), \quad (1)$$

where X is defined as

$$X = \frac{\beta\Delta p_0}{1 - \beta\Delta p_0} \left(\frac{R}{L}\right). \quad (2)$$

Taking into account the compressibility of the SBR as well as the high-pressure drop of about 700 bar during the capillary experiments,

Denn¹⁶ proposed the following equation to estimate the temperature increase during the process, which is known as viscous heating:

$$\left(\beta + \frac{1}{\rho C_V}\right) \Delta p_0 = e^{\Delta T} - e^{-\beta\Delta p} \rightarrow \Delta T = \ln\left[\left(\beta + \frac{1}{\rho C_V}\right) \Delta p_0 + e^{-\beta\Delta p}\right], \quad (3)$$

where ρ is the density of samples at the temperature of the experiment and C_V is the heat capacity. For SBR, $\rho = 0.96 \times 10^3\text{ kg m}^{-3}$ at 100°C and $C_V = 1.6 \times 10^3\text{ J kg}^{-1}\text{ K}^{-1}$.¹⁹

To compare the model that predicts the temperature increase [Eq. (3)], the simple power law model, Eq. (4), suggested by Bird *et al.* is used.²⁰ The following equation has been used in numerous studies^{21–23} to predict the temperature increase in extrusion dies due to viscous heating:

$$\Delta T = \frac{\rho}{k} \left(\frac{nR}{3n+1}\right)^2 \left[\left(\frac{n+1}{n}\right) \left(\frac{V}{R}\right)\right]^{n+1}, \quad (4)$$

where k is the thermal conductivity ($k = 0.22 \times 10^3\text{ kg mm s}^{-2}\text{ K}^{-1}$ for SBR¹⁹), n is the power law exponent of the flow curve, and $\sigma = K\dot{\gamma}^n$.

IV. RESULTS AND DISCUSSION

A. Investigation of molecular architecture via Mark-Houwink analysis

Figure 2 presents the Mark-Houwink (MH)^{24,25} plot, i.e., the intrinsic viscosity, $[\eta]$, as a function of the molecular weight, M_w , to investigate the molecular architecture (linear, branched, etc.) of the three investigated SBRs. The Mark-Houwink analysis was performed by comparing the intrinsic viscosity $[\eta]$, obtained by the viscometer of the size exclusion chromatography (SEC), as a function of molecular weight of the studied SBRs obtained by multi-angle laser light

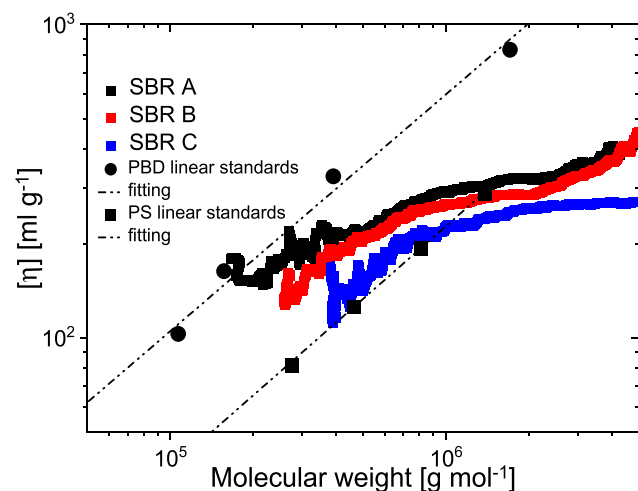


FIG. 2. The intrinsic viscosity $[\eta]$ as a function of molar mass as obtained via MALLS. The black circles and squares are calibration standards of homopolymer polybutadiene and polystyrene with linear molecular architecture, respectively. The deviation of the SBRs from the linear trend after 600 kg mol^{-1} indicates branched molecular architecture.

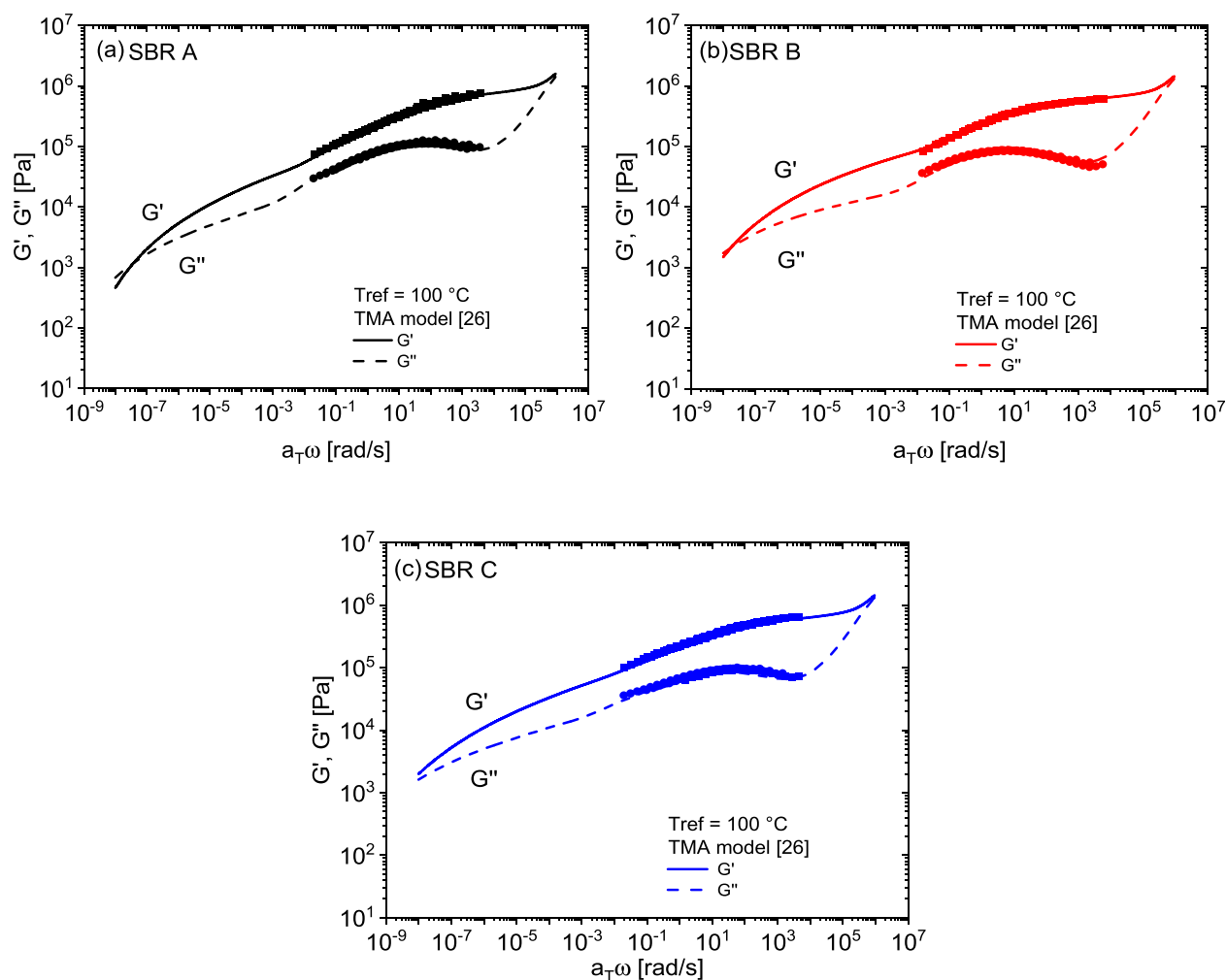


FIG. 3. The master curves of the linear viscoelastic moduli (the storage G' and loss G'' modulus) of investigated SBRs samples at $T_{ref}=100\text{ }^{\circ}\text{C}$: (a) SBR A, (b) SBR B, and (c) SBR C. The master curves are fitted by the constitutive model of van Ruymbeke *et al.*²⁶ in order to estimate the zero-shear viscosity of the samples. The fitted molecular parameters for the constitutive modeling are listed in Table III.

scattering (MALLS). Homopolymer polybutadiene (PBD) and polystyrene (PS) standards with linear architecture were used to compare them with the experimental data of the three SBRs. It can be observed from Fig. 2 that the experimental data of the investigated SBRs deviate from the linear trend of the calibration standards. The reduction of the intrinsic viscosity begins at $\sim 600\text{ kg mol}^{-1}$ for all of three investigated SBRs. The increased deviation for all the three SBR samples as the molecular weight increases from the calibration standards implies that the molecular architecture is branched or is a mixture of linear and branched molecules at molecular weights $M_w > 600\text{ kg mol}^{-1}$.

B. Linear viscoelasticity and molecular architecture analysis

Figures 3(a)–3(c) depict the master curves of the storage modulus (G'), loss modulus (G''), and magnitude of complex viscosity ($|\eta^*(\omega)|$) of all three SBR compounds at the reference temperature of

$T_{ref}=100\text{ }^{\circ}\text{C}$. Due to the elastomeric nature of these compounds, the terminal relaxation has not been reached. In order to predict the terminal relaxation and the zero-shear viscosity from the limited experimental data, constitutive modeling has been performed. Specifically, the Time-Marched Algorithm (TMA) developed by van Ruymbeke *et al.*²⁶

TABLE III. Input fitting parameters for the TMA model of van Ruymbeke *et al.*²⁶ at $T_{ref}=100\text{ }^{\circ}\text{C}$.

Name	Linear M_w (kg mol^{-1})	\mathcal{D} (-)	G_N^0 (kPa)	τ_e (s)	ϕ_{linear} (%)	ϕ_{star} (%)	M_e (kg mol^{-1})
SBR A	180	2.7	800	4×10^{-6}	0.4	0.6	3100
SBR B	160	1.7	650	5×10^{-6}	0.3	0.7	2900
SBR C	165	2.8	650	5×10^{-6}	0.2	0.8	2900

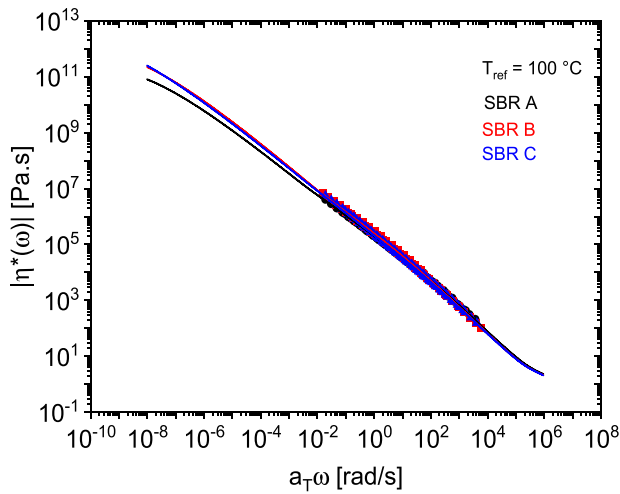


FIG. 4. Master curves of the magnitude of complex viscosity for all the investigated SBRs. The fitted parameters of the constitutive model²⁶ that best describe the experimental data are listed in Table III.

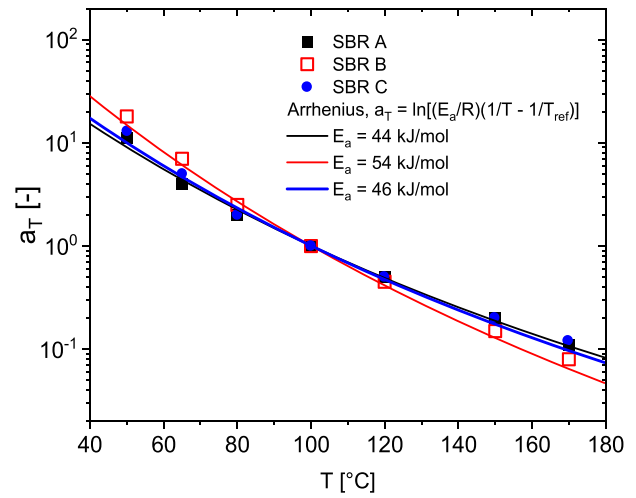


FIG. 5. Horizontal shift factors a_T obtained by the construction of master curves of storage G' and loss G'' moduli as a function of temperature. The shift factors a_T are fitted by the Arrhenius equation, and the activation energy of each of the investigated samples is obtained (listed in the figure).

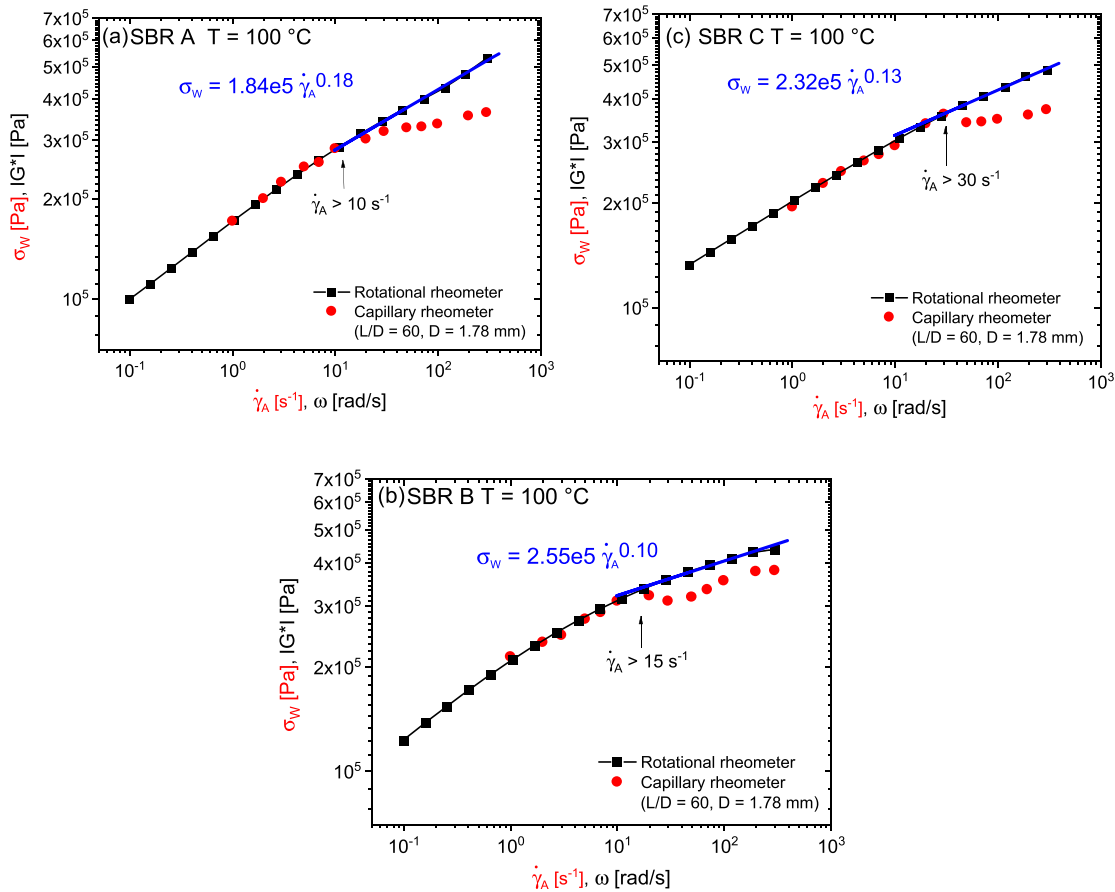


FIG. 6. Wall shear stress (red circles) as a function of apparent shear rate obtained by a round capillary die with $L/D = 60$ and $D = 1.78$ mm and magnitude of complex modulus (black squares) as a function of angular frequency at $T = 100$ °C. Deviations of these two curves are due to wall slip.

has been used (tube-based model). This constitutive model is able to describe the flow behavior of polymeric melts of linear and star (branched) molecular architecture. Since the detailed molecular architecture of the random branched SBRs is not known, it is assumed that these polymers are mixtures of linear and branched chains, which in fact is supported by the experimental results discussed in Figs. 1 and 2. The model needs the estimated volumetric fraction ϕ of linear and star (branched) segments, the plateau modulus G_N^0 , the characteristic entanglement relaxation time (equilibration time) τ_e , and the estimated molar mass of the backbone and branch (arm) as input parameters. The input parameters of the TMA model that best fit the experimental data [continuous lines in Figs. 3(a)–3(c)] are listed in Table III.

The selection of the molar mass for the polymer backbone was obtained by the molar mass distribution (MWD) shown in Fig. 1. To ensure simplicity in the model fitting, it was assumed that the M_w and M_n for both linear and star chains were identical, in order to minimize the number of fitted variables. The choice of M_w was made to align with the magnitude observed in the GPC data (Table I), with the trends for M_w and polydispersity aligning with the experimental results for the three SBRs. Since the Rouse dynamics have not been reached based on the experimental data, τ_e was strategically chosen to coincide with the plateau region for the loss modulus, and also following the trend of τ_e in relation to the glass transition temperature for the three polymers (Table II). The intrinsic viscosity deviations from the calibration values, as shown in Fig. 2, guided the determination of the percentage of linear chains, which was set lower than that of branched chains. This percentage followed a decreasing trend for SBR A, SBR B, and SBR C. Considering the entanglement molecular weight (M_e) for SBR with 25 wt. % of styrene according to Fetters *et al.*²⁷ and Mark *et al.*,¹⁹ M_e was established as 2900 g mol^{-1} for SBR B and SBR C. However, due to the higher styrene percentage in SBR A, its M_e was set to a higher value.

Apart from the estimated difference in their molecular architecture (Fig. 2) and estimated molecular weight listed in Table III, the investigated SBRs have rather similar molecular architecture and flow behavior within the processing region (Fig. 4). The experimental results of Figs. 3 and 4 represent master curves of storage modulus (G'), loss modulus (G''), and magnitude of complex viscosity ($|\eta^*(\omega)|$) obtained from a wide temperature range between 50 and 170°C . The horizontal shift factors, a_T , needed to construct the master curves presented in Fig. 3 at the reference temperature of 100°C follow the Arrhenius equation: $a_T = \ln[(E_a/R)(1/T - 1/T_{ref})]$, where E_a is the flow-activation energy. In Fig. 5, the a_T values as a function of temperature are presented. SBR A and SBR C have similar activation energy of about $E_a = 44$ and $E_a = 46 \text{ kJ mol}^{-1}$, respectively, compared to that of SBR B of $E_a = 54 \text{ kJ mol}^{-1}$. The difference in the activation energy may occur due to the different microstructure composition (Table II). The level of branching and breadth of the molecular weight distribution affect the activation energy.²⁸ However, since the differences in molar mass dispersity (Fig. 1 and Table I), branching (Fig. 2 and Table III), and energy of activation are relatively small, the available analysis cannot conclusively distinguish definite differences between the molecular architecture of these SBR compounds. As already discussed, they all contain some portion of branched chains (SBR C more branched than the others) with similar flow properties.

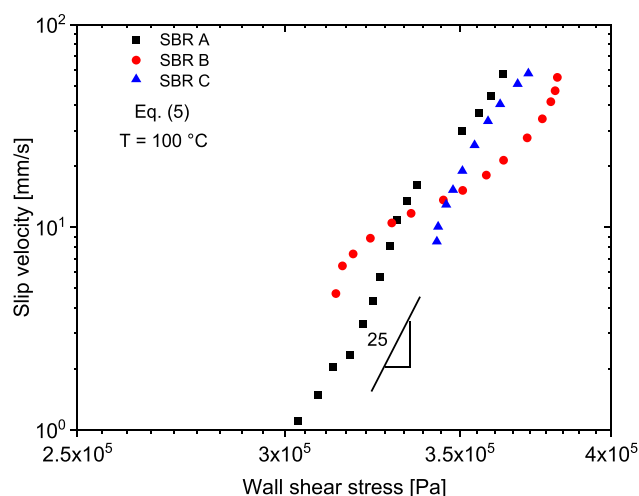


FIG. 7. Slip velocity as a function of wall shear stress for the investigated samples. Slip velocities are calculated by Eq. (5). Experimental data are obtained by a round capillary die with $L/D = 60$ and $D = 1.78 \text{ mm}$ at $T = 100^\circ\text{C}$.

V. CAPILLARY EXTRUSION

A. The flow curves

Capillary extrusion experiments were carried out in order to obtain the flow curves of the three SBR samples, i.e., the wall shear stress (σ_w) as a function of apparent shear rate ($\dot{\gamma}_A$) (Fig. 6). For the capillary experiments, a single capillary die having diameter $D = 1.78 \text{ mm}$ and length of $L = 106.8 \text{ mm}$ was used, so $L/D = 60$. Due to the high L/D ratio used, the true wall shear stress can be directly obtained without the need of Bagley (entry pressure) correction as mentioned earlier.¹⁵

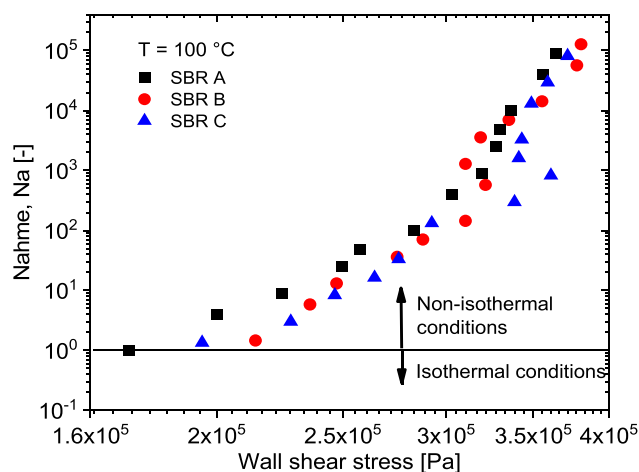


FIG. 8. The dimensionless Nahme number, Na , as a function of the wall shear stress in capillary extrusion of the investigated samples at the operating temperature of $T = 100^\circ\text{C}$. The experiments were performed with a capillary die with geometrical characteristics, $L/D = 60$, $D = 1.78 \text{ mm}$. Na exceeds 1 in all cases and thus non-isothermal conditions exist.

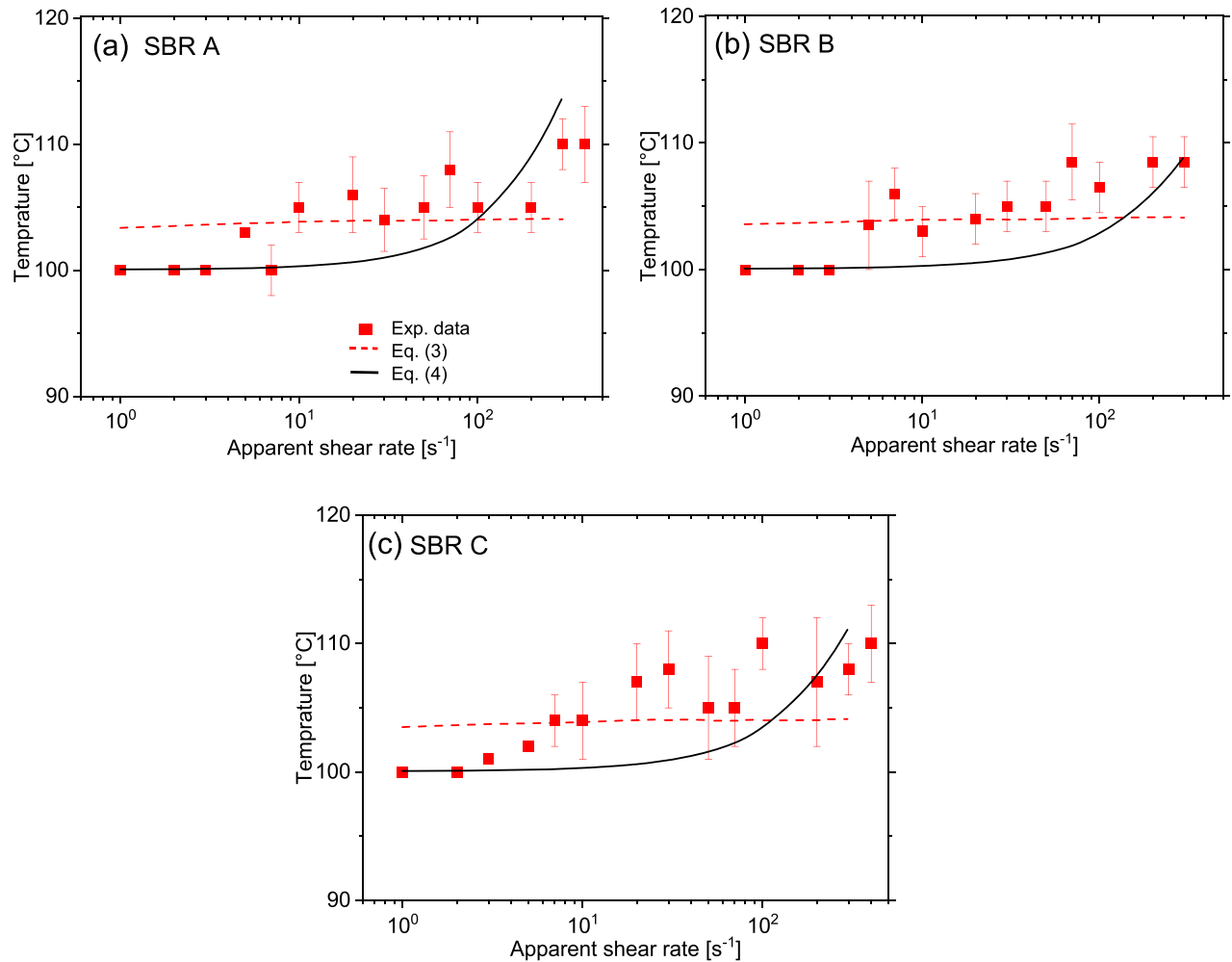


FIG. 9. Measured temperature (red solid square) at the exit of the extrusion die with a thermocouple as a function a shear rate. The dash red line is the theoretical prediction of the Denn model, Eq. (3),¹⁶ and the solid black line is the power law model, Eq. (4).^{20–23}

The extrusion temperature was set at $T = 100^\circ\text{C}$. Figure 6 depicts the flow curves of all three SBR compounds from capillary rheometry together with the linear viscoelastic data (the magnitude of complex modulus $|G^*|$ as a function of angular frequency ω). The experimental data plotted in Fig. 6 imply that the Cox–Merz rule is approximately valid up to apparent shear rates of about $\dot{\gamma}_A = 10\text{ s}^{-1}$ for SBR A, up to $\dot{\gamma}_A = 15\text{ s}^{-1}$ for SBR B, and up to $\dot{\gamma}_A = 30\text{ s}^{-1}$ for SBR C. The deviation of the steady capillary data from the linear viscoelasticity (LVE) is due to the presence of wall slippage.¹

B. Slip velocity calculations

In order to estimate the slip velocity, the following equation¹ is used:

$$V_s = \frac{D}{8} \left(\dot{\gamma}_A - \frac{4n}{3n+1} \omega \right), \quad (5)$$

where V_s is the slip velocity and n is the local slope of the linear viscoelasticity (LVE) flow curve, i.e., $n = d(\log |G^*|)/d(\log \omega)$. The factor

$\frac{4n}{3n+1}$ transforms the angular frequency (rad/s), ω , to an apparent shear rate under no-slip conditions, using Cox–Merz⁹ law.

Figure 7 plots the slip velocity of the three compounds calculated by means of Eq. (5). The slip velocities for all the investigated SBR samples exhibit a strong dependency on the wall shear stress. Specifically, the slip velocity has a power law dependency of the wall shear stress, with a scaling exponent up to 25 indicating nearly plug flow once slip is initiated. Due to the overlapping molecular weight distribution (MWD), as shown in Fig. 1, there is no clear correlation between the weight average molar mass M_w , the dispersity index \mathcal{D} , and the slip velocity V_s .

C. Viscous heating effects

Due to high pressures (up to 10^6 Pa) during capillary extrusion and high apparent shear rates (10^2 – 10^3 s^{-1}), significant amount of mechanical energy is dissipated into heat and, therefore, the temperature rises, thus rendering the flow non-isothermal. The dimensionless Nahme number, Na ,^{18,21} is the critical parameter for estimating the

importance of viscous heating. It quantifies how much the temperature increase will affect the viscosity and, therefore, the level of stress. For flow in a capillary, Na can be written as follows:

$$Na \equiv \frac{V^2 \eta_0}{\kappa T_0}, \quad (6)$$

where κ is the polymer thermal conductivity ($\kappa = 0.22 \times 10^3 \text{ kg mm s}^{-2} \text{ K}^{-1}$),¹⁹ η_0 is the zero-shear viscosity, and T_0 is the reference temperature. Since the investigated SBRs have not reached the terminal flow regime (Fig. 3), the zero-shear viscosity cannot be determined, which is needed in Eq. (6). In the present analysis, we use a value for $\eta_0 \geq 10^9 \text{ Pa s}$ (see Fig. 4). Thus, Na values as a function of the wall shear stress for the three investigated SBRs are plotted in Fig. 8. As seen, Na is greater than 1 as the wall shear stress exceeds in most cases $\sim 2 \times 10^5 \text{ Pa}$. Thus, viscous heating is significant rendering

non-isothermal conditions. Hence, the extrusion temperature setting of $T = 100^\circ \text{C}$ can only be considered operational and the measurements should be corrected for non-isothermal effects in order to estimate the proper slip velocities of the three compounds at the fixed reference temperature of $T = 100^\circ \text{C}$.

To demonstrate experimentally the non-isothermal conditions, a thermocouple was used to measure the temperature of the melt at the die exit. The results are presented in Fig. 9 for the three SBR samples. The experimental results confirm that there is a gradual temperature increase up to 10°C with increase in the shear rate. The model predictions of Eq. (3),¹⁶ and the power law model, Eq. (4),^{20–23} are included in Fig. 9. The prediction of Eq. (3) is based on the theoretical adiabatic conditions. Equation (3) predicts a difference of about 25 bar from the measured pressure, considering the effect of pressure on viscosity. This leads to a theoretical temperature increase in about $\sim 5^\circ \text{C}$ over the

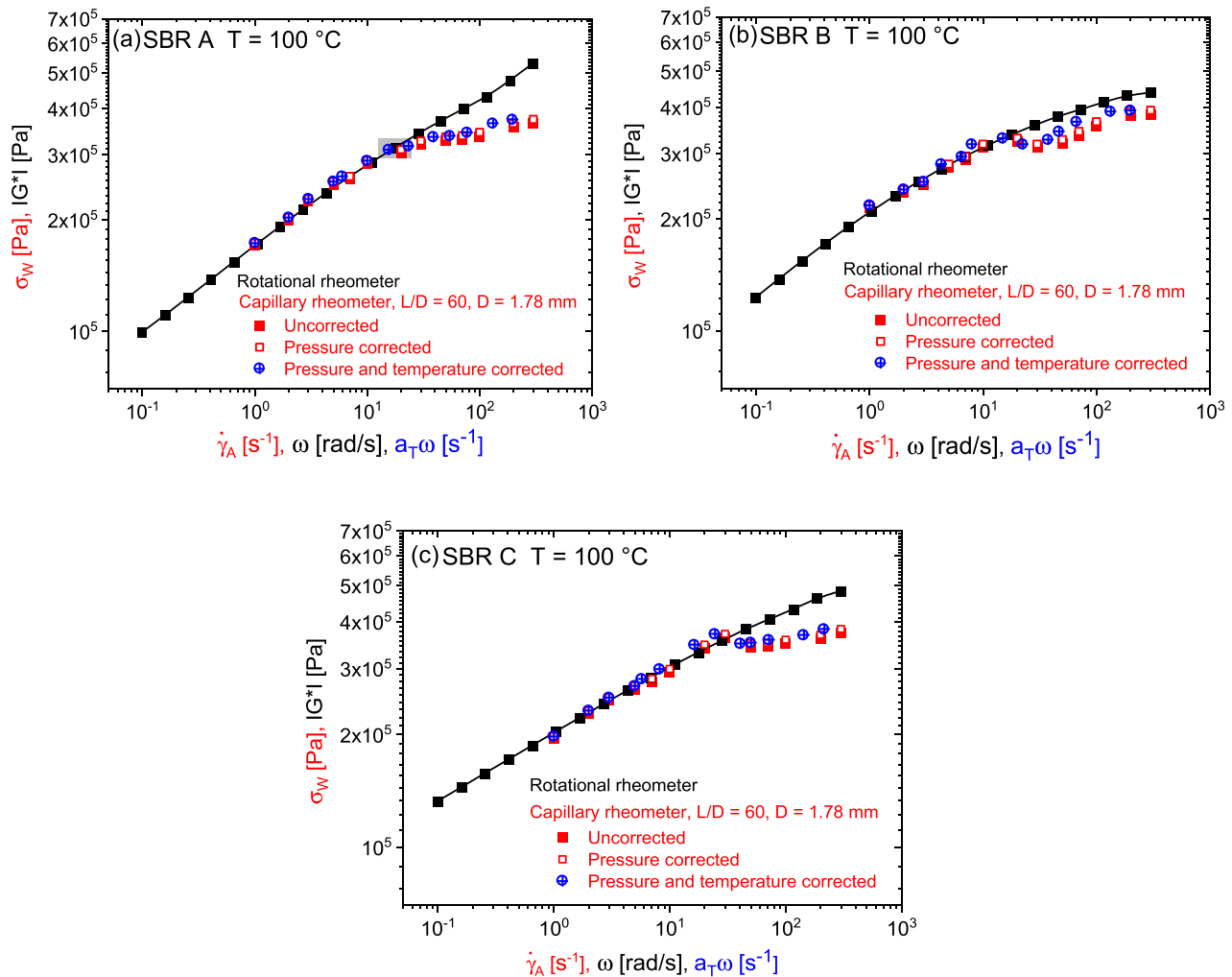


FIG. 10. Magnitude of complex modulus as a function of angular frequency (solid black squares). Wall shear stress (solid red squares) and pressure-corrected wall shear stress (open red squares) as a function of apparent shear rate. Pressure- and thermal-corrected wall shear stress (open blue circles) as a function of shifted apparent shear rate. The pressure-corrected data have 3%–5% higher values than raw data. The pressure- and thermal-corrected data are shifted to the lower shear rates depending on the a_T shift factor for each investigated sample. The raw data are obtained by a round capillary die with $L/D = 60$ and $D = 1.78 \text{ mm}$ at $T_{\text{theoretical}} = 100^\circ \text{C}$.

wide range of shear rates from 1 to $3 \times 10^2 \text{ s}^{-1}$. The experimental data are better described by the power law model, Eq. (4), showing similar trends with the experimental temperature increase with shear rate. Due to the scaling of the Nahme number, $Na \sim V^2$, the temperature is expected to increase non-linearly with shear rate. These experimental results can be used now to account for the viscous heating effects in order to calculate the corrected slip velocity of the rubbers.

D. Calculating the viscous heating-corrected slip velocity

Based on the above-mentioned experimental results, the following methodology is suggested to correct the capillary experimental data for the viscous heating effects in order to correct the slip velocity calculation presented in Fig. 7. The methodology presented below assumes that the time-temperature superposition (tTS) principle²⁹ applies to obtain the master curves of the linear viscoelastic moduli of

the polymers (Figs. 3 and 4), that Na is greater than 1, and that non-isothermal conditions are present (see Fig. 7).

The proposed methodology is as follows:

- (1) Correct the capillary data for the effect of pressure by using Eq. (1). This takes into account the effect of pressure on viscosity based on the dimensions of the capillary die.
- (2) Correct the pressure-corrected data for viscous dissipation effects by using the experimentally measured temperatures on the extrusion die exit and the shift factors a_T determined by the tTS principle.
- (3) Use the corrected data and Eq. (5) to calculate the new slip velocities, which now refer to the operating temperature.

Based on the above-described methodology, Fig. 10 presents the wall shear stress as a function of apparent shear rate in three different versions. First, the filled red squares are the raw data (uncorrected) obtained directly from the capillary rheology experiments, same as

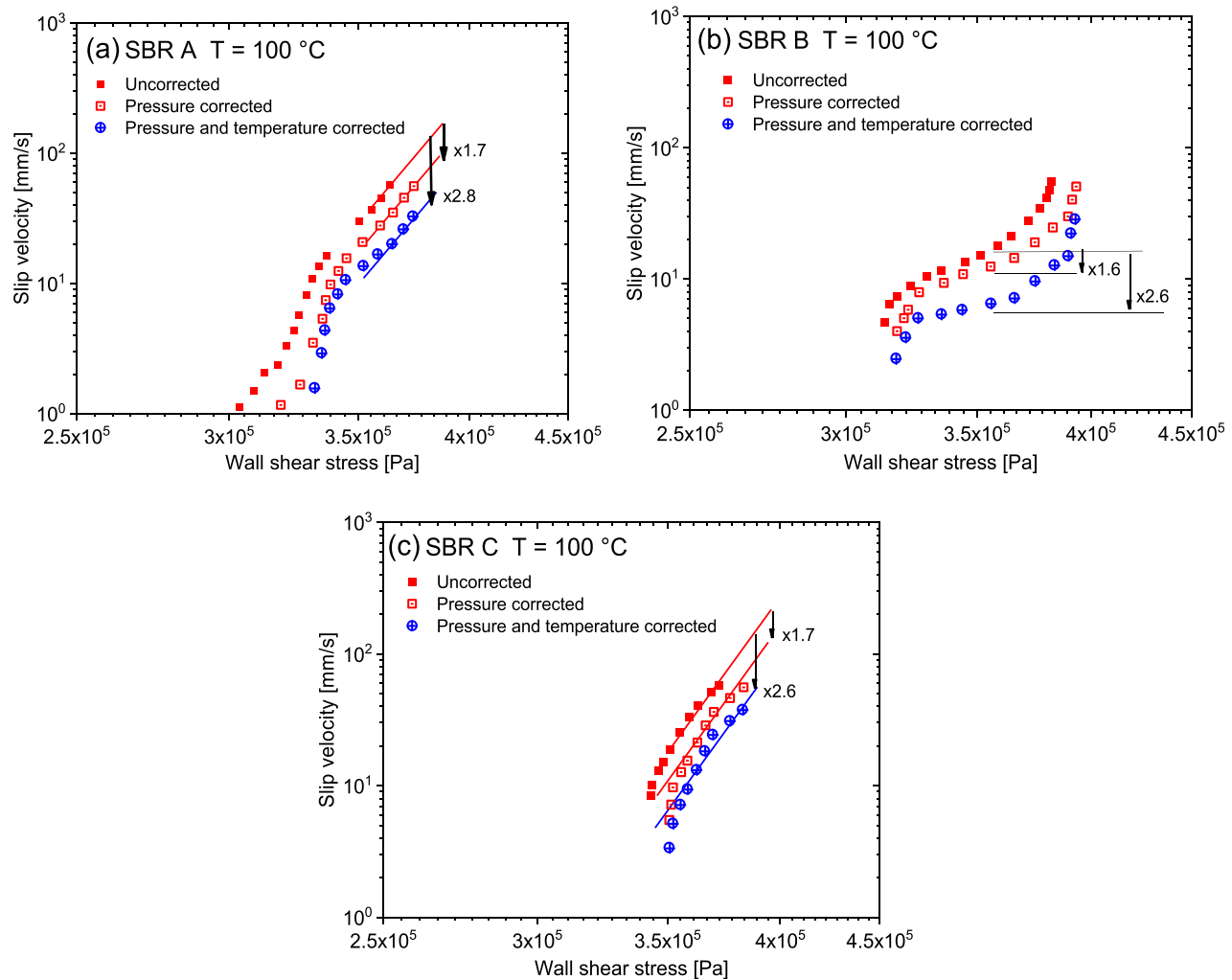


FIG. 11. Slip velocity as a function of wall shear stress for the investigated samples. Slip velocities are calculated by Eq. (5). The slip velocities are corrected from pressure and viscous heating influence. The experimental data are obtained by a round capillary die with $L/D = 60$ and $D = 1.78 \text{ mm}$.

those presented in Fig. 6. Second, the open red squares present the pressure-corrected wall shear stress data by using Eq. (1). Practically speaking, this correction moves vertically upward the wall shear stress data by about $\sim 3\%$. Third, the blue open circles represent the thermally corrected data based on the tTS principal. Since the specific extrusion temperature on the die exit is recorded by the thermocouple and the tTS principal is valid, the horizontal shifting factors a_T are obtained and the corresponding data are corrected accordingly.

The slip velocities, presented in Fig. 11, have been calculated using Eq. (5) on the three different sets of data shown in Fig. 10 (red squares—raw data, open red squares—pressure-corrected data, and blue open circles—thermal-corrected data). The same symbols as in Fig. 11, the pressure correction influences the slip velocity by a factor of up to 1.7, and the viscous heating effect influences the slip velocity by a factor of 2.8. Without such corrections, misleading results may be obtained on the slip velocities obtained directly from the raw experimental data. Nevertheless, the trend of the slip velocity as a function of wall shear stress remains similar for all the three different set of data.^{30,31}

VI. CONCLUSIONS

The findings from this study are significant for quantifying the slip velocity of elastomers for process optimization. By developing the suggested methodology to correct the slip velocities for pressure and viscous heating effects, a better understanding and additional insights of the capillary flow of elastomers are gained. These insights can be leveraged by compound and extrusion engineers to assess and optimize the extrusion performance, improve die design, improve computational simulations, and optimize processing conditions for thermal-sensitive compounds (i.e., compounds with curing agents). In summary, the following conclusions can be drawn:

- (i) During the extrusion of rubber materials, in the present case SBR, the temperature on the extrusion die exit might increase up to 10°C from the temperature set at the instrument due to significant viscous dissipation.
- (ii) Even though the rubber materials have significantly low compressibility factor, and their viscosity seems not to be affected by pressure, the small 3% difference on the pressure after the compressibility correction may affect the slip velocity calculation by a factor of up to 1.7, due to the nonlinear dependence of the slip velocity on wall shear stress.
- (iii) In an elastomeric compound with no curing agents, such as neat SBRs, the 10°C temperature rise at the die exit might seem negligible. However, this temperature increase may influence the slip velocity by a factor of up to 2.8, due to the significant dependence of the viscosity on temperature (relatively large energy of activation).

ACKNOWLEDGMENTS

The authors thank Karlsruhe House of Young Scientists (KHYS) for the financial support and Pirelli Tyre S. p. A. for commercial sample support and for the permission to publish this work. The authors would also like to thank the fruitful discussions and support from AiF-iGF 19925N project.

AUTHOR DECLARATIONS

Conflict of Interest

The authors have no conflicts to disclose.

Author Contributions

Christos K. Georgantopoulos: Conceptualization (equal); Data curation (equal); Investigation (equal); Methodology (equal); Validation (equal). **Ziyue Zhang:** Data curation (equal); Formal analysis (equal); Software (equal). **Michael A. Pollard:** Formal analysis (equal); Supervision (equal). **Andrea Causa:** Resources (equal); Supervision (equal); Validation (equal). **Roland Kadar:** Supervision (equal); Validation (equal). **Manfred Wilhelm:** Conceptualization (equal); Methodology (equal); Supervision (equal). **Evelyn van Ruymbeke:** Investigation (equal); Software (equal). **Savvas G. Hatzikiriakos:** Conceptualization (equal); Supervision (equal).

DATA AVAILABILITY

The data that support the findings of this study are available within the article.

REFERENCES

- ¹M. Mooney, "Explicit formulas for slip and fluidity," *J. Rheol.* **2**, 210–222 (1931).
- ²S. G. Hatzikiriakos, "Wall slip of molten polymers," *Prog. Polym. Sci.* **37**, 624–643 (2012).
- ³Ph. Mourniac, J. F. Agassant, and B. Verges, "Determination of the wall slip velocity in the flow of a SBR compound," *Rheol. Acta* **31**, 565–574 (1992).
- ⁴A. Ya. Malkin, A. V. Baranov, and M. E. Vickulenkova, "Experimental estimation of wall slip of filler rubbers compounds," *Rheol. Acta* **32**, 150–155 (1993).
- ⁵J. M. Lupton and R. W. Regehr, "Melt flow of polyethylene at high rates," *Polym. Eng. Sci.* **5**, 235–242 (1965).
- ⁶A. V. Ramamurthy, "Wall slip in viscous fluids and influence of materials of construction," *J. Rheol.* **30**, 337–357 (1986).
- ⁷E. E. Rosenbaum and S. G. Hatzikiriakos, "Wall slip in the capillary flow of molten polymers subject to viscous heating," *AIChE J.* **43**, 598–608 (1997).
- ⁸C. K. Shih, *Capillary Extrusion and Mold Flow Characteristics of an Incompatible Blend of Two Elastomers* (Science and Technology of Polymer Processing, MIT Press, Cambridge, 1979), pp. 528–539.
- ⁹W. P. Cox and E. H. Merz, "Correlation of dynamic and steady flow viscosities," *J. Polym. Sci.* **28**, 619 (1958).
- ¹⁰H. H. Winter, "Three views of viscoelasticity for Cox–Merz materials," *Rheol. Acta* **48**, 241 (2009).
- ¹¹H. H. Winter, "Viscous dissipation in shear flows of molten polymers," *Adv. Heat Transfer* **13**, 205–267 (1977).
- ¹²H. W. Cox and C. W. Macosko, "Viscous dissipation in die flows," *AIChE J.* **20**, 785–795 (1974).
- ¹³S. Soltani and F. A. Sourki, "Effect of carbon black type on viscous heating, heat build-up, and relaxation behaviour of SBR compounds," *Iran. Polym. J.* **14**, 745–751 (2005).
- ¹⁴P. Heyer, C. Wurm, and H. Ehrentauf, *Measurement and Visualization of Slip in Rubber Flow* (AERC, Seville, ES, 2022).
- ¹⁵J. M. Dealy and J. Wang, *Melt Rheology and Its Application in the Plastic Industry*, 2nd ed. (Springer Science + Business Media, Dordrecht, 2013).
- ¹⁶M. M. Denn, "Pressure drop-flow rate equation for adiabatic capillary flow with a pressure- and temperature-dependent viscosity," *Polym. Eng. Sci.* **21**, 65–68 (1981).
- ¹⁷H. Winter and M. Mours, "The cyber infrastructure initiative for rheology," *Rheol. Acta* **45**, 331–338 (2006).
- ¹⁸J. M. Dealy and K. F. Wissbrun, *Melt Rheology and Its Role in Plastics Processing* (Van Nostrand Reinhold, New York, 1990).

- ¹⁹J. Mark, *Physical Properties of Polymer Handbook*, 2nd ed. (Springer, New York, 2007).
- ²⁰R. B. Bird, R. C. Armstrong, and O. Hassager, *Dynamics of Polymeric Liquids, Vol. 1: Fluid Mechanics*, 2nd ed. (Wiley, New York, 1987).
- ²¹M. Ansari, T. Zisis, S. G. Hatzikiriakos, and E. Mitsoulis, "Capillary flow of low-density polyethylene," *Polym. Eng. Sci.* **52**, 476–699 (2012).
- ²²E. Mitsoulis, S. S. Abdali, and N. C. Markatos, "Flow simulation of Herschel-Bulkley fluids through extrusion dies," *Can. J. Chem. Eng.* **71**, 147–160 (1993).
- ²³G. Barakos and E. Mitsoulis, "Non-isothermal viscoelasticity simulations of extrusion thought dies and prediction of the bending phenomenon," *J. Non-Newtonian Fluid Mech.* **62**, 55–79 (1996).
- ²⁴W. Burchard, *Branched Polymers II. Advances in Polymer Science* (Springer, Berlin, 1999), Vol. 143.
- ²⁵J. Brandrup, E. H. Immergut, and E. A. Grulke, *Polymer Handbook*, 4th ed. (John Wiley & Sons, New York, 1999).
- ²⁶E. van Ruymbeke, R. Keunings, and C. Bailly, "Prediction of linear viscoelastic properties mixtures of entangled star and linear polymers: Modified tube-based model and comparison with experimental results," *J. Non-Newtonian Fluid Mech.* **128**, 7–22 (2005).
- ²⁷L. J. Fetters, D. J. Lohse, S. T. Milner, and W. W. Graessley, "Packing length influence in linear polymer melts on the entanglement, critical, and reptation molecular weights," *Macromolecules* **32**, 6847 (1999).
- ²⁸S. G. Hatzikiriakos, "Long chain branching and polydispersity effects on the rheological properties of polyethylenes," *Polym. Eng. Sci.* **40**, 2279–2287 (2000).
- ²⁹R. Li, "Time-temperature superposition method for glass transition temperature of plastic materials," *Mat. Sci. Eng. A* **278**, 36–45 (2000).
- ³⁰C. K. Georgantopoulos, M. K. Esfahani, C. Botha, M. A. Pollard, I. F. C. Naue, A. Causa, R. Kádár, and M. Wilhelm, "Modeling the spatial characteristics of extrusion flow instabilities for styrene-butadiene rubbers: Investigation the influence of molecular weight distribution, molecular architecture and temperature," *Phys. Fluids* **33**, 93108 (2021).
- ³¹C. K. Georgantopoulos, M. K. Esfahani, C. Botha, I. F. C. Naue, N. Dingenouts, A. Causa, R. Kádár, and M. Wilhelm, "Mechano-optical characterization of extrusion flow instabilities in styrene-butadiene rubbers: Investigation the influence of molecular properties and die geometry," *Macromol. Mater. Eng.* **306**, 2000801 (2021).